Int. J. Solids Structures Vol. 24, No. 6, pp. 637–656, 1988
Printed in Great Britain.

0020-7683/88 $3.00 + .00

A HYPERCIRCLE METHOD OF FRAME ANALYSIS—II. PRACTICE†

C. A. NELSON
Honeywell Inc., 7225 Northland Drive, Brooklyn Park, MN 55428, U.S.A.

and

L. E. GOODMAN‡
Civil and Mineral Engineering Department, University of Minnesota, Minneapolis, MN 55455, U.S.A.

(*Received* 14 *January* 1987; *in revised form* 13 *November* 1987)

Abstract—The hypercircle method of structural analysis, the theory of which was developed in Part I, is shown to have certain advantages, in terms of computer time required, over conventional methods of analysis for very large rigid-jointed planar frames. This efficiency is achieved by the systematic use of "superelements" based on the four-node rectangular finite element.

INTRODUCTION

In the preceding paper[1], the hypercircle method of Synge and Prager was used to derive formulae bounding displacements and internal forces in rigid-jointed frames. For complex structures with many members the dimensionality of the function subspaces encountered in these formulae is large, presenting an obstacle to practical utilization of the hypercircle method. In this paper that obstacle is removed by introduction of special linear subspaces based on interpolation procedures borrowed from the finite element method. This technique, which may be termed the superelement method, provides an effective tool for the analysis of large rectangular rigid-jointed frames subjected to lateral loads.

Figure 1(a) shows the type of structure and loading considered. While not the most general possible rectangular frame, it is adequate to exhibit the practical potentialities of the hypercircle method. The bays of this frame are numbered $\alpha = 1, b$ and have lengths L_α. The stories are numbered $i = 1, n(\alpha)$ and have heights H_i. The pair (α, i) thus identifies a "cell" of the structure. The joints are labelled using the same system except that α now refers to the column line and i to the beam line; hence $\alpha = 1, b+1$ and $i = 1, c(\alpha)$, where $c(\alpha) = \max[n(\alpha-1), n(\alpha)]$. Associated naturally with this scheme is the system of beam and column identification shown in Fig. 1(b).

THE BASIC COMPATIBLE STATES AND THE KINEMATICAL EQUATIONS

The basic compatible states (i.e. those defining the subspace L') that will be used here are those corresponding to the individual joint displacements. In order to represent these states and their inner products it is convenient to introduce a descriptive notation in place of the generalized notation used in Ref. [1]. Thus $\mathbf{U}_i^\alpha$ will denote the state obtained by imposing a unit horizontal displacement on the joint labelled (α, i) while all other displacements are prevented. Similarly $\boldsymbol{\theta}_i^\alpha$ and $\mathbf{V}_i^\alpha$ will correspond to a unit rotation and vertical displacement of the joint, respectively. The joint displacements and forces associated with these states are shown in Fig. 2. Deformation due to shear is ignored. Since $\mathbf{S}_0^* = \mathbf{0}$, a general state $\mathbf{S}^* \in \mathbf{L}^*$ may be represented

† Equations are numbered consecutively from Part I[1].
‡ Author to whom correspondence should be addressed.

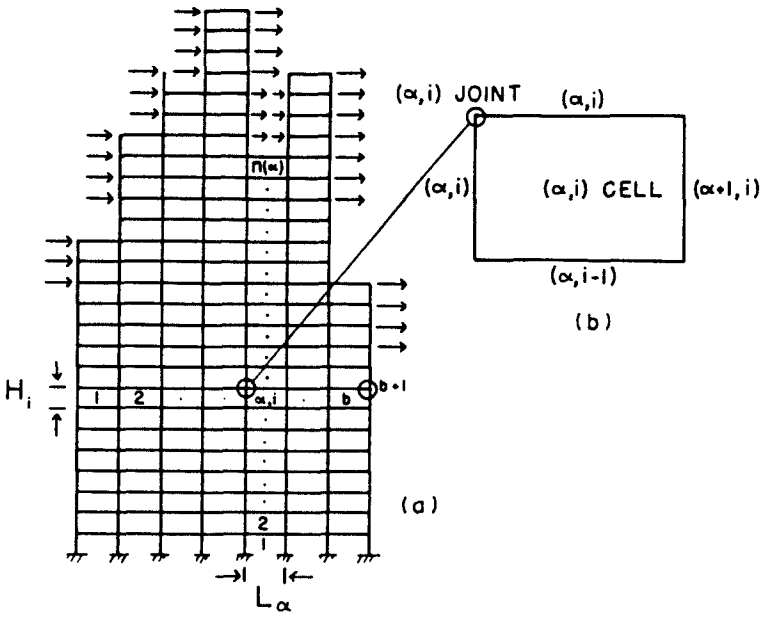

Fig. 1. General structure and loading.

$$\mathbf{S}^* = \sum_{\alpha=1}^{b+1} \sum_{i=1}^{c(\alpha)} [u_i^\alpha \mathbf{U}_i^\alpha + \theta_i^\alpha \boldsymbol{\theta}_i^\alpha + v_i^\alpha \mathbf{V}_i^\alpha]. \tag{93}$$

If this expression is used to rederive the displacement equations, eqns (48), then the latter may be rewritten as

$$\sum_{\beta=1}^{b+1} \sum_{j=1}^{c(\beta)} \mathbf{K}_{ij}^{\alpha\beta} \mathbf{x}_j^\beta = \mathbf{P}_i^\alpha \qquad \alpha = 1, b+1; \quad i = 1, c(\alpha) \tag{94}$$

where

$$\mathbf{K}_{ij}^{\alpha\beta} = \begin{bmatrix} \langle \mathbf{U}_i^\alpha, \mathbf{U}_j^\beta \rangle & \langle \mathbf{U}_i^\alpha, \boldsymbol{\theta}_j^\beta \rangle & \langle \mathbf{U}_i^\alpha, \mathbf{V}_j^\beta \rangle \\ \langle \boldsymbol{\theta}_i^\alpha, \mathbf{U}_j^\beta \rangle & \langle \boldsymbol{\theta}_i^\alpha, \boldsymbol{\theta}_j^\beta \rangle & \langle \boldsymbol{\theta}_i^\alpha, \mathbf{V}_j^\beta \rangle \\ \langle \mathbf{V}_i^\alpha, \mathbf{U}_j^\beta \rangle & \langle \mathbf{V}_i^\alpha, \boldsymbol{\theta}_j^\beta \rangle & \langle \mathbf{V}_i^\alpha, \mathbf{V}_j^\beta \rangle \end{bmatrix} \tag{95}$$

$$\mathbf{x}_j^\beta = [u_j^\beta \quad \theta_j^\beta \quad v_j^\beta]^T \tag{96}$$

$$\mathbf{P}_i^\alpha = [\langle \mathbf{S}_0^{**}, \mathbf{U}_i^\alpha \rangle \quad \langle \mathbf{S}_0^{**}, \boldsymbol{\theta}_i^\alpha \rangle \quad \langle \mathbf{S}_0^{**}, \mathbf{V}_i^\alpha \rangle]^T. \tag{97}$$

The inner products in matrix (95) are obtained using eqn (41) and Fig. 2. Since each interior joint is connected to four other joints as well as to itself it follows from eqn (94) that

$$\mathbf{K}_{ii}^{\alpha(\alpha-1)} \mathbf{x}_i^{\alpha-1} + \mathbf{K}_{i(i-1)}^{\alpha\alpha} \mathbf{x}_{i-1}^\alpha + \mathbf{K}_{ii}^{\alpha\alpha} \mathbf{x}_i^\alpha + \mathbf{K}_{i(i+1)}^{\alpha\alpha} \mathbf{x}_{i+1}^\alpha + \mathbf{K}_{ii}^{\alpha(\alpha+1)} \mathbf{x}_i^{\alpha+1} = \mathbf{P}_i^\alpha \tag{98}$$

may be written for each interior joint (a, i), together with appropriate equations for the boundary joints. The matrices appearing in eqn (98) are, in general, tridiagonal.

For future reference, it is noted that the "bandwidth" of matrix $\mathbf{K}$ represented in eqn (98) is minimized by interchanging the order of the summation in eqn (94), i.e.

$$\sum_{j=1}^{n_{\max}} \sum_{\beta(j)} \mathbf{K}_{ij}^{\alpha\beta} \mathbf{x}_j^\beta = \mathbf{P}_i^\alpha \qquad i = 1, n_{\max}; \quad \alpha = \alpha(i). \tag{99}$$

Here $n_{\max}$ is the maximum number of stories over all the bays of the frame, and $\beta(j)$ denotes

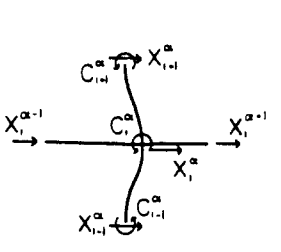

$$X_i^{\alpha-1} = -K_i^{\alpha-1}$$
$$X_{i-1}^{\alpha} = -12\,g_i^{\alpha}$$
$$C_{i-1}^{\alpha} = 6\,g_i^{\alpha}H_i$$
$$X_i^{\alpha} = K_i^{\alpha-1} + K_i^{\alpha} + 12\,(g_{i+1}^{\alpha} + g_i^{\alpha})$$
$$C_i^{\alpha} = 6\,(g_i^{\alpha}H_i - g_{i+1}^{\alpha}H_{i+1})$$
$$X_{i+1}^{\alpha} = 12\,g_{i+1}^{\alpha}$$
$$C_{i+1}^{\alpha} = -6\,g_{i+1}^{\alpha}H_{i+1}$$
$$X_i^{\alpha+1} = -K_i^{\alpha}$$

$$K_i^{\alpha} = EA_{bi}^{\alpha}/L_{\alpha} \qquad k_i^{\alpha} = EA_{ci}^{\alpha}/H_i$$
$$G_i^{\alpha} = EI_{bi}^{\alpha}/L_{\alpha}^3 \qquad g_i^{\alpha} = EI_{ci}^{\alpha}/H_i^3$$

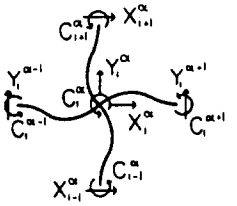

$$Y_i^{\alpha-1} = G_i^{\alpha-1}L_{\alpha-1}$$
$$C_i^{\alpha-1} = 2\,G_i^{\alpha-1}L_{\alpha-1}^2$$
$$X_{i-1}^{\alpha} = -6\,g_i^{\alpha}H_i$$
$$C_{i-1}^{\alpha} = 2\,g_i^{\alpha}H_i^2$$
$$X_i^{\alpha} = 6\,(g_i^{\alpha}H_i^{\alpha} - g_{i+1}^{\alpha}H_{i+1})$$
$$Y_i^{\alpha} = 6\,(G_i^{\alpha}L_{\alpha} - G^{\alpha-1}L_{\alpha-1})$$
$$C_i^{\alpha} = 4\,(g_i^{\alpha}H_i^2 + g_{i+1}^{\alpha}H_{i+1}^2 + G_i^{\alpha-1}L_{\alpha}^2 + G_i^{\alpha}L_{\alpha}^2)$$
$$X_{i+1}^{\alpha} = 6\,g_{i+1}^{\alpha}H_{i+1}$$
$$C_{i+1}^{\alpha} = 2\,g_{i+1}^{\alpha}H_{i+1}^2$$
$$Y_i^{\alpha+1} = -6\,G_i^{\alpha}L_{\alpha}$$
$$C_i^{\alpha+1} = 2\,G_i^{\alpha}L_{\alpha}^2$$

Fig. 2. Joint displacements and forces associated with U_i^x and θ_i^x.

those column lines that intersect the jth beam line. This has the effect of changing the order of the terms in eqn (98). If the order of summation is unimportant, the Einstein summation convention may be used to suppress the summation signs. Then the equation

$$\mathbf{K}_{ij}^{x\beta}\mathbf{x}_j^{\beta} = \mathbf{P}_i^x \tag{100}$$

may represent either eqn (94) or eqn (99).

Since the frame is loaded only by horizontal forces at the joints, the vector $\mathbf{P}_i^x$ is given by

$$\langle \mathbf{S}_0^{**}, \mathbf{U}_i^x \rangle = P_i^x; \quad \langle \mathbf{S}_0^{**}, \boldsymbol{\theta}_i^x \rangle = \langle \mathbf{S}_0^{**}, \mathbf{V}_i^x \rangle = 0 \tag{101}$$

where P_i^x is the lateral load at the joint (α, i).

SUPERELEMENTS

The equations developed in the preceding section are now transformed by defining a linear subspace of much smaller dimension than the actual number of kinematical degrees of freedom of the structure. This is done by defining a new set of displacements and a linear transformation between the new and original set, i.e. a relation of the form of eqns (86). The particular form of this relation used here is based upon the rectangular four-node finite element.

The first step in the implementation of the procedure is the construction of a kinematical superelement mesh. This is done by dividing the frame, along its beam and column lines, into rectangular four-node elements, the nodes coinciding with the joints that lie at the

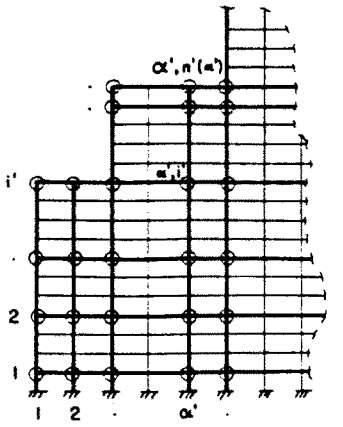

Fig. 3. Portion of typical kinematical superelement mesh.

corners of the rectangles. An example of a mesh constructed in this way is shown in Fig. 3. The nodes are specified by pairs (α', i'), where $\alpha' = 1, b'$ and $i' = 1, n'(\alpha')$.

It is well known from finite element analysis that the displacement field within the rectangular element with corner nodes may be related to the nodal displacements by means of bilinear interpolation[2]. The discrete analogue of this is used to relate the joint displacements within a superelement to the displacements of the corner joints. Then if nodal displacements are denoted by

$$\mathbf{x}_i^{\alpha} = [u_i^{\alpha} \quad \theta_i^{\alpha} \quad v_i^{\alpha}]^{\mathrm{T}} \tag{102}$$

the full set of joint displacements is given by

$$\mathbf{x}_i^{\alpha} = \sum_{\alpha'=1}^{b'} \sum_{i'=1}^{n'(\alpha')} \Gamma_{ii'}^{\alpha\alpha'} \mathbf{x}_{i'}^{\alpha'} \qquad \alpha = 1, b+1; \quad i = 1, c(\alpha). \tag{103}$$

In the above equation $\Gamma_{ii'}^{\alpha\alpha'}$ are the matrices of two-dimensional shape functions obtained by multiplying the one-dimensional linear shape functions in the horizontal and vertical directions, i.e.

$$\Gamma_{ii'}^{\alpha\alpha'} = N_{ii'} N^{\alpha\alpha'} \tag{104}$$

where

$$N_{ii'} = \begin{cases} 0 & i \leqslant i(i'-1) \\ [i - i(i'-1)]/[i(i') - i(i'-1)] & i(i'-1) \leqslant i \leqslant i(i') \\ [i(i'+1) - i]/[i(i'+1) - i(i')] & i(i') \leqslant i \leqslant i(i'+1) \\ 0 & i \geqslant i(i'+1) \end{cases} \tag{105}$$

$$N^{\alpha\alpha'} = \begin{cases} 0 & \alpha \leqslant \alpha(\alpha'-1) \\ [\alpha - \alpha(\alpha'-1)]/[\alpha(\alpha') - \alpha(\alpha'-1)] & \alpha(\alpha'-1) \leqslant \alpha \leqslant \alpha(\alpha') \\ [\alpha(\alpha'+1) - \alpha]/[\alpha(\alpha'+1) - \alpha(\alpha')] & \alpha(\alpha') \leqslant \alpha \leqslant \alpha(\alpha'+1) \\ 0 & \alpha \geqslant \alpha(\alpha'+1). \end{cases} \tag{106}$$

In eqns (105) and (106), $\alpha(\alpha')$ denotes the number of the column line corresponding to the vertical nodal line numbered α' and $i(i')$ the number of the beam line corresponding to the horizontal nodal line numbered i'.

It is noted that the interpolation is carried out on the beam and column indices rather than by actual distances. This assumes that floor heights and column line spacings are

approximately constant within any one element; the superelement mesh should be constructed accordingly.

THE VERTEX EQUATIONS

Equations (103), with $\Gamma_{ii'}^{\alpha\alpha'}$ defined by eqns (105) and (106) for any given kinematical superelement mesh, represent the desired linear transformations. The vertex of the linear subspace defined by these equations is determined by the vertex equations

$$\underline{\mathbf{K}}\underline{\mathbf{x}} = \underline{\mathbf{P}}. \tag{107}$$

This may be written out more explicitly in the form of eqns (94), i.e.

$$\sum_{\beta'=1}^{b'} \sum_{j'=1}^{n'(\beta')} \underline{\mathbf{K}}_{i'j'}^{\alpha'\beta'} \underline{\mathbf{x}}_{j'}^{\beta'} = \underline{\mathbf{P}}_{i'}^{\alpha'} \qquad \alpha' = 1, b'; \quad i' = 1, n'(\alpha') \tag{108}$$

where $\underline{\mathbf{K}}_{i'j'}^{\alpha'\beta'}$ are 3×3 matrices. In order to obtain $\underline{\mathbf{K}}$ and $\underline{\mathbf{P}}$, invariance principle (88) is applied. Thus

$$\underline{\mathbf{K}}\underline{\mathbf{x}} \cdot \underline{\mathbf{x}} - 2\underline{\mathbf{P}} \cdot \underline{\mathbf{x}} = \mathbf{K}\mathbf{x} \cdot \mathbf{x} - 2\mathbf{P} \cdot \mathbf{x}. \tag{109}$$

This may be written as

$$\mathbf{K}_{i'j'}^{\alpha'\beta'} \mathbf{x}_{j'}^{\beta'} \cdot \mathbf{x}_{i'}^{\alpha'} - 2\mathbf{P}_{i'}^{\alpha'} \cdot \mathbf{x}_{i'}^{\alpha'} = \mathbf{K}_{ij}^{\alpha\beta} \mathbf{x}_j^{\beta} \cdot \mathbf{x}_i^{\alpha} - 2\mathbf{P}_i^{\alpha} \cdot \mathbf{x}_i^{\alpha} \tag{110}$$

where the Einstein summation convention is understood. If transformation (103) is substituted into the right-hand side of the above equation, there follows

$$\mathbf{K}_{i'j'}^{\alpha'\beta'} = \Gamma_{ii'}^{\alpha\alpha'} \mathbf{K}_{ij}^{\alpha\beta} \Gamma_{jj'}^{\beta\beta'}; \quad \mathbf{P}_{i'}^{\alpha'} = \Gamma_{ii'}^{\alpha\alpha'} \mathbf{P}_i^{\alpha}. \tag{111}$$

Equations (111) correspond to transformations (89).

The structure of the vertex equations is now examined. It is observed that each interior node is connected through the surrounding elements to all of the eight surrounding nodes. Equation (108) may therefore be put into the form of eqn (98). For each interior node (α', i') the equation

$$\begin{aligned} &\underline{\mathbf{K}}_{i'(i'-1)}^{\alpha'(\alpha'-1)} \underline{\mathbf{x}}_{(i'-1)}^{(\alpha'-1)} + \underline{\mathbf{K}}_{i'i'}^{\alpha'(\alpha'-1)} \underline{\mathbf{x}}_{i'}^{(\alpha'-1)} + \underline{\mathbf{K}}_{i'(i'+1)}^{\alpha'(\alpha'-1)} \underline{\mathbf{x}}_{(i'+1)}^{(\alpha'-1)} + \underline{\mathbf{K}}_{i'(i'-1)}^{\alpha'\alpha'} \underline{\mathbf{x}}_{(i'-1)}^{\alpha'} \\ &+ \underline{\mathbf{K}}_{i'i'}^{\alpha'\alpha'} \underline{\mathbf{x}}_{i'}^{\alpha'} + \underline{\mathbf{K}}_{i'(i'+1)}^{\alpha'\alpha'} \underline{\mathbf{x}}_{(i'+1)}^{\alpha'} + \underline{\mathbf{K}}_{i'(i'-1)}^{\alpha'(\alpha'+1)} \underline{\mathbf{x}}_{(i'-1)}^{(\alpha'+1)} + \underline{\mathbf{K}}_{i'i'}^{\alpha'(\alpha'+1)} \underline{\mathbf{x}}_{i'}^{(\alpha'+1)} + \underline{\mathbf{K}}_{i'(i'+1)}^{\alpha'(\alpha'+1)} \underline{\mathbf{x}}_{(i'+1)}^{(\alpha'+1)} = \underline{\mathbf{P}}_{i'}^{\alpha'} \end{aligned} \tag{112}$$

may be written, together with a set of equations for the nodes lying on the boundary of the frame. Now from the form of transformation (111) it may be deduced that each of the nine 3×3 matrices appearing in eqn (112) is in general tridiagonal. For computational purposes it is again noted that the bandwidth of the vertex equations is minimized by rewriting eqn (108)

$$\sum_{j'=1}^{b'_{\max}} \sum_{\beta'(j')} \underline{\mathbf{K}}_{i'j'}^{\alpha'\beta'} \underline{\mathbf{x}}_{j'}^{\beta'} = \underline{\mathbf{P}}_{i'}^{\alpha'} \qquad i' = 1, b'_{\max}; \quad \alpha' = \alpha'(i') \tag{113}$$

where $b'_{\max}$ is the maximum number of "superstories" over all the "superbays" of the mesh and $\beta'(j')$ denotes those vertical nodal lines that intersect the jth horizontal nodal line.

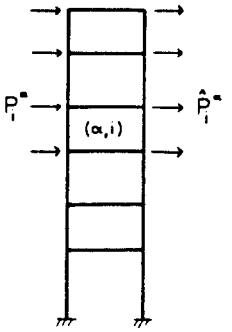

Fig. 4. Lateral forces acting on typical bay.

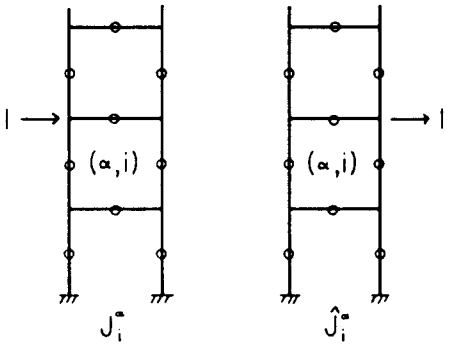

Fig. 5. Loading for states $\mathbf{J}_i^x$ and $\hat{\mathbf{J}}_i^x$.

THE STATICAL EQUATIONS

The statical problem is now considered. It may be broken down into two parts: (i) the construction of the state $\mathbf{S}_0^{**} \in L^{**}$ and computations thereupon; (ii) the definition of the subspace L'' through a suitable set of residual states and the construction of the flexibility matrix $\mathbf{B}$ of their inner products. The latter part is made easier by introducing residual states that cause $\mathbf{B}$ to assume a form corresponding exactly to the form of the stiffness matrix $\mathbf{K}$, which has already been described. These states will be developed later. First, the state $\mathbf{S}_0^{**}$ is constructed.

CONSTRUCTION OF $\mathbf{S}_0^{**}$

It is assumed that the structure is loaded as shown in Fig. 1(a); i.e. lateral forces act on all the horizontal faces. Due to the uneven roofline, a given bay may be subjected to forces on both sides; these are labelled P_i^x and $\hat{P}_i^x$ (Fig. 4). Let each bay in turn be disconnected from the adjoining bays by severing the connecting beams and let the resulting single bay be rendered statically determinate by inserting mid-member hinges as in the earlier example. The member forces produced by the lateral loads acting on the determinate structure may be developed with the aid of the two loading systems shown in Fig. 5. Let $\mathbf{J}_i^x$ and $\hat{\mathbf{J}}_i^x$ be the states obtained when a unit load is applied to the upper left and upper right corner, respectively, of the (α, i) cell. Then state $\mathbf{S}_0^{**}$ may be written as

$$\mathbf{S}_0^{**} = \sum_{\alpha=1}^{b} \sum_{i=1}^{n(\alpha)} (P_i^x \mathbf{J}_i^x + \hat{P}_i^x \hat{\mathbf{J}}_i^x). \tag{114}$$

The member forces associated with $\mathbf{J}_i^x$ and $\hat{\mathbf{J}}_i^x$ are not developed explicitly. Instead, these two states are written in terms of the new states

$$\mathbf{D}_i^x = (4/H_i)(\mathbf{J}_i^x + \hat{\mathbf{J}}_{i-1}^x), \quad \hat{\mathbf{D}}_i^x = (4/H_i)(\mathbf{J}_i^x - \hat{\mathbf{J}}_i^x). \tag{115}$$

Equation (114) may now be written as

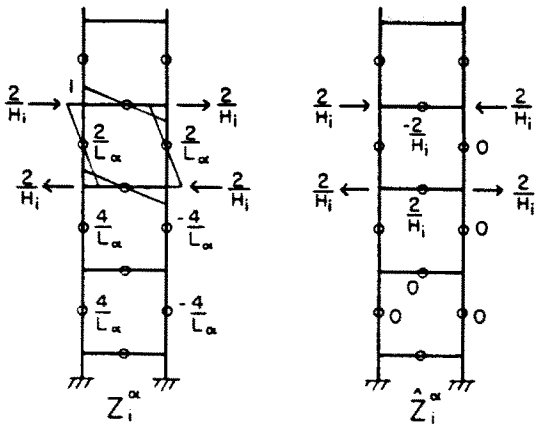

Fig. 6. Loading and member forces for states $\mathbf{Z}_i^\alpha$ and $\hat{\mathbf{Z}}_i^\alpha$.

$$\mathbf{S}_0^{**} = \frac{1}{4}\sum_{\alpha=1}^{b}\sum_{i=1}^{n(\alpha)}\left[P_i^\alpha\sum_{k=1}^{i}H_k\mathbf{D}_k^\alpha + \hat{P}_i^\alpha\sum_{k=1}^{i}H_k\hat{\mathbf{D}}_k\right]. \tag{116}$$

But

$$\sum_{i=1}^{n(\alpha)}P_i^\alpha\sum_{k=1}^{i}H_k\mathbf{D}_k^\alpha = \sum_{i=1}^{n(\alpha)}H_i\mathbf{D}_i^\alpha\sum_{k=i}^{n(\alpha)}P_k^\alpha = \sum_{i=1}^{n(\alpha)}H_i\Pi_i^\alpha\mathbf{D}_i^\alpha \tag{117}$$

where

$$\Pi_i^\alpha = \sum_{k=i}^{n(\alpha)}P_k^\alpha \tag{118}$$

is the sum of all the loads acting on the left side of the αth bay from the ith story level to the top. Similarly

$$\sum_{i=1}^{n(\alpha)}P_i^\alpha\sum_{k=1}^{i}H_k\mathbf{D}_k^\alpha = \sum_{i=1}^{n(\alpha)}H_i\hat{\Pi}_i^\alpha\hat{\mathbf{D}}_i^\alpha \tag{119}$$

$$\hat{\Pi}_i^\alpha = \sum_{k=i}^{n(\alpha)}\hat{P}_k^\alpha. \tag{120}$$

Hence eqn (116) may be written as

$$\mathbf{S}_0^{**} = \frac{1}{4}\sum_{\alpha=1}^{b}\sum_{i=1}^{n(\alpha)}H_i(\Pi_i^\alpha\mathbf{D}_i^\alpha + \hat{\Pi}_i^\alpha\hat{\mathbf{D}}_i^\alpha). \tag{121}$$

Representation (121) may be used to carry out computations involving $\mathbf{S}_0^{**}$, but these are simpler if the two linear combinations

$$\mathbf{Z}_i^\alpha = \tfrac{1}{2}(\mathbf{D}_i^\alpha + \hat{\mathbf{D}}_i^\alpha), \quad \hat{\mathbf{Z}}_i^\alpha = \tfrac{1}{2}(\mathbf{D}_i^\alpha - \hat{\mathbf{D}}_i^\alpha) \tag{122}$$

are introduced. These are shown in Fig. 6. Equation (121) then becomes

$$\mathbf{S}_0^{**} = \frac{1}{4}\sum_{\alpha=1}^{b}\sum_{i=1}^{n(\alpha)}H_i(q_i^\alpha\mathbf{Z}_i^\alpha + \hat{q}_i^\alpha\hat{\mathbf{Z}}_i^\alpha) \tag{123}$$

where

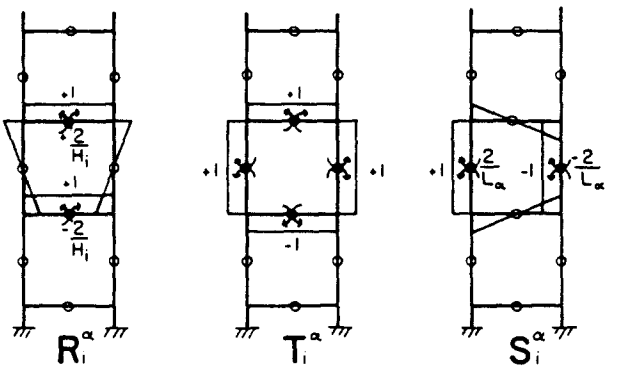

Fig. 7. Basic residual states.

$$q_i^x = \Pi_i^x + \hat{\Pi}_i^x, \quad \hat{q}_i^x = \Pi_i^x - \hat{\Pi}_i^x. \tag{124}$$

From eqn (123), a computation shows that

$$16\|\mathbf{S}_0^{**}\|^2 = \sum_{x=1}^{b} \sum_{\beta=1}^{b} \sum_{i=1}^{n(x)} \sum_{j=1}^{n(\beta)} H_i H_j [W_{ij}^{x\beta} q_i^x q_j^\beta + \hat{W}_{ij}^{x\beta} \hat{q}_i^x \hat{q}_j^\beta] \tag{125}$$

where

$$W_{ij}^{x\beta} = \langle \mathbf{Z}_i^x, \mathbf{Z}_j^\beta \rangle, \quad \hat{W}_{ij}^{x\beta} = \langle \hat{\mathbf{Z}}_i^x, \hat{\mathbf{Z}}_j^\beta \rangle. \tag{126}$$

Expression (125) provides a convenient means of computing $\|\mathbf{S}_0^{**}\|$. In applying this formula advantage may be taken of the bandedness of matrix $W_{ij}^{x\beta}$ and the extreme sparseness of $\hat{W}_{ij}^{x\beta}$. The components of these matrices are obtained easily upon reference to Fig. 6.

THE BASIC RESIDUAL STATES AND THE STATICAL EQUATIONS

The basic residual states (i.e. those defining subspace L'') are developed by again considering each bay of the frame in turn as a statically determinate unit with hinges at the mid-points of all the members. Since three degrees of statical indeterminacy (three statical DOFs) are associated with each story of a single bay frame, it is necessary to construct three independent residual states for each cell of the structure. The most natural choice of these states, by virtue of their symmetry properties and localized nature, are the three states $\mathbf{R}_i^x$, $\mathbf{T}_i^x$ and $\mathbf{S}_i^x$ shown in Fig. 7. These may be constructed by applying various combinations of unit moment pairs at the hinges of the (x, i) cell, as shown in the figures. It is noted that the generalized notation of eqn (42) has been replaced by a more descriptive notation.

A general state $\mathbf{S}^{**} \in L^{**}$ may now be represented

$$\mathbf{S}^{**} = \mathbf{S}_0^{**} + \sum_{x=1}^{b} \sum_{i=1}^{n(x)} (r_i^x \mathbf{R}_i^x + t_i^x \mathbf{T}_i^x + s_i^x \mathbf{S}_i^x). \tag{127}$$

Quantities r_i^x, t_i^x, s_i^x may be termed the "redundants" of the (x, i) cell. If representation (127) is used to rederive the force equations, eqns (48), it may be written as

$$\sum_{\beta=1}^{b} \sum_{j=1}^{n(\beta)} \mathbf{B}_{ij}^{x\beta} \boldsymbol{\sigma}_j^\beta + \Delta_i^x = \mathbf{0} \qquad x = 1, b; \quad j = 1, n(\beta) \tag{128}$$

where

$$\mathbf{B}_{ij}^{\alpha\beta} = \begin{bmatrix} \langle \mathbf{R}_i^\alpha, \mathbf{R}_j^\beta \rangle & \langle \mathbf{R}_i^\alpha, \mathbf{T}_j^\beta \rangle & \langle \mathbf{R}_i^\alpha, \mathbf{S}_j^\beta \rangle \\ \langle \mathbf{T}_i^\alpha, \mathbf{R}_j^\beta \rangle & \langle \mathbf{T}_i^\alpha, \mathbf{T}_j^\beta \rangle & \langle \mathbf{T}_i^\alpha, \mathbf{S}_j^\beta \rangle \\ \langle \mathbf{S}_i^\alpha, \mathbf{R}_j^\beta \rangle & \langle \mathbf{S}_i^\alpha, \mathbf{T}_j^\beta \rangle & \langle \mathbf{S}_i^\alpha, \mathbf{S}_j^\beta \rangle \end{bmatrix} \tag{129}$$

$$\boldsymbol{\sigma}_j^\beta = [r_j^\beta \quad t_j^\beta \quad s_j^\beta]^{\mathrm{T}} \tag{130}$$

$$\Delta_i^\alpha = [\langle \mathbf{S}_0^{**}, \mathbf{R}_i^\alpha \rangle \quad \langle \mathbf{S}_0^{**}, \mathbf{T}_i^\alpha \rangle \quad \langle \mathbf{S}_0^{**}, \mathbf{S}_i^\alpha \rangle]^{\mathrm{T}}. \tag{131}$$

The inner products in matrix (129) are obtained from definition (18) and Fig. 7. If the pattern of inner products contained therein is examined, a useful analogy emerges. With the correspondence

$$\mathbf{U} \leftrightarrow \mathbf{R}, \quad \boldsymbol{\theta} \leftrightarrow \mathbf{T}, \quad \mathbf{V} \leftrightarrow \mathbf{S} \tag{132}$$

matrices $\mathbf{K}_{ij}^{\alpha\beta}$ in eqn (94) and $\mathbf{B}_{ij}^{\alpha\beta}$ in eqn (129) are seen to be exactly analogous. In the statical formulation, however, the cell replaces the joint as the basic entity. Since the same connectivity properties apply to both entities, eqn (128) may be written, by analogy with eqn (98), as

$$\mathbf{B}_{ii}^{\alpha(\alpha-1)}\boldsymbol{\sigma}_i^{\alpha-1} + \mathbf{B}_{i(i-1)}^{\alpha\alpha}\boldsymbol{\sigma}_{i-1}^{\alpha} + \mathbf{B}_{ii}^{\alpha\alpha}\boldsymbol{\sigma}_i^{\alpha} + \mathbf{B}_{i(i+1)}^{\alpha\alpha}\boldsymbol{\sigma}_{i+1}^{\alpha} + \mathbf{B}_{ii}^{\alpha(\alpha+1)}\boldsymbol{\sigma}_i^{\alpha+1} + \Delta_i^\alpha = \mathbf{0}. \tag{133}$$

The above equation may be written for each interior cell (α, i), together with similar equations that apply to the boundary cells. The matrices appearing in eqn (133) are tridiagonal, with the same pattern that occurs in eqn (98). Finally, by analogy with eqn (99), the bandwidth of $\mathbf{B}$ is minimized by rewriting eqn (128)

$$\sum_{j=1}^{n_{\max}} \sum_{\beta(j)} \mathbf{B}_{ij}^{\alpha\beta}\boldsymbol{\sigma}_j^\beta + \Delta_i^\alpha = \mathbf{0} \qquad i = 1, n_{\max}; \quad \alpha = \alpha(i) \tag{134}$$

where $\beta(j)$ now ranges over those bays that extend to the jth story level.

It is now necessary to consider the vector Δ_i^α defined by eqn (131). From eqn (123)

$$\begin{aligned} \langle \mathbf{S}_0^{**}, \mathbf{R}_i^\alpha \rangle &= \frac{1}{4} \sum_{\beta=1}^{b} \sum_{j=1}^{n(\beta)} (\langle \mathbf{R}_i^\alpha, \mathbf{Z}_j^\beta \rangle H_j q_j^\beta = \langle \mathbf{R}_i^\alpha, \mathbf{Z}_j^\beta \rangle H_j q_j^\beta) \\ \langle \mathbf{S}_0^{**}, \mathbf{T}_i^\alpha \rangle &= 0 \\ \langle \mathbf{S}_0^{**}, \mathbf{S}_i^\alpha \rangle &= \frac{1}{4} \sum_{\beta=1}^{b} \sum_{j=1}^{n(\beta)} \langle \mathbf{S}_i^\alpha, \mathbf{Z}_j^\beta \rangle H_j q_j^\beta. \end{aligned} \tag{135}$$

The inner products appearing in the above equations are obtained from the member forces shown in Fig. 7 upon application of definition (18). Also reflected in eqns (135) are the vanishing inner products

$$\langle \mathbf{T}_i^\alpha, \mathbf{Z}_j^\beta \rangle = \langle \mathbf{T}_i^\alpha, \mathbf{Z}_j^\beta \rangle = \langle \mathbf{S}_i^\alpha, \mathbf{Z}_j^\beta \rangle = 0. \tag{136}$$

STATICAL SUPERELEMENTS AND THE VERTEX EQUATIONS

Given the previous development of the kinematical superelement mesh as a means of reducing the number of degrees of freedom of the structure, it is now natural to try to construct a statical mesh for the same purpose. Since in the statical formulation the cell merely replaces the joint as the basic entity, the nature of the statical superelement mesh is

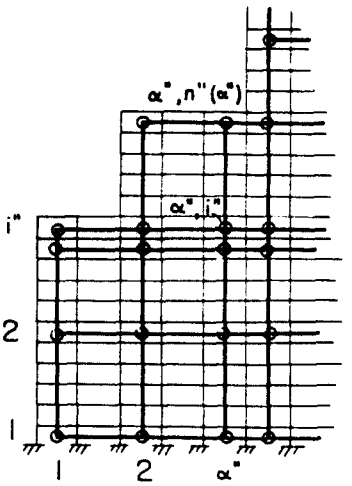

Fig. 8. Portion of typical statical superelement mesh.

readily apparent. An example of such a mesh is shown in Fig. 8. It is seen that the rectangular four-node elements span between cells of the frame rather than between joints. Hence a set of nodal redundants is defined

$$\underline{\sigma}_{i''}^{\alpha''} = [\underline{r}_{i''}^{\alpha''} \quad \underline{t}_{i''}^{\alpha''} \quad \underline{s}_{i''}^{\alpha''}]^{\mathrm{T}}. \tag{137}$$

These give the full set of cell redundants through the bilinear interpolation

$$\sigma_{i''}^{\alpha''} = \sum_{\alpha''=1}^{b''} \sum_{i''=1}^{n''(\alpha'')} \Omega_{ii''}^{\alpha\alpha''} \underline{\sigma}_{i''}^{\alpha''} \qquad \alpha = 1, b; \quad i = 1, n(\alpha). \tag{138}$$

These equations are analogous to eqn (103). The matrix $\Omega_{ii''}^{\alpha\alpha''}$ is given by

$$\Omega_{ii''}^{\alpha\alpha''} = N_{i}\cdot N^{\alpha\alpha''} \tag{139}$$

where the shape functions on the right are given by eqns (105) and (106) with i'' in place of i' and α'' in place of α'. It is important to note that while the kinematical and statical superelement meshes are based upon the same interpolation concept, they need not in principle represent similar discretizations of the structure.

It is now a simple matter to write down the statical vertex equations. They are, compactly

$$\mathbf{B}\underline{\sigma} + \underline{\Delta} = \mathbf{0} \tag{140}$$

or, more explicitly, by analogy with eqn (107)

$$\mathbf{B}_{i''j''}^{\alpha''\beta''}\underline{\sigma}_{j''}^{\beta''} + \underline{\Delta}_{i''}^{\alpha''} = \mathbf{0} \tag{141}$$

in which $\mathbf{B}_{i''j''}^{\alpha''\beta''}$ are 3×3 matrices given by

$$\mathbf{B}_{i''j''}^{\alpha''\beta''} = \Omega_{ii''}^{\alpha\alpha''}\mathbf{B}_{ij}^{\alpha\beta}\Omega_{jj''}^{\beta\beta''} \tag{142}$$

and

$$\underline{\Delta}_{i''}^{\alpha''} = \Omega_{ii''}^{\alpha\alpha''}\Delta_{i}^{\alpha}. \tag{143}$$

In the above equations the summation convention is understood. Transformations (142)

and (143) correspond to eqns (89). The previously discussed bandwidth considerations apply also to eqn (141).

BOUNDS ON THE STRAIN ENERGY

With the solutions $\underline{x}$ and $\underline{\sigma}$ of the kinematical and statical vertex equations, bounds on the strain energy of the solution may be obtained. From eqns (58) and (92)

$$\|\mathbf{S}\|^2 \geqslant \|\mathbf{V}^*\|^2 = \underline{\mathbf{P}}_i^{x^T} \cdot \underline{\mathbf{x}}_i^x \tag{144}$$

and

$$\|\mathbf{S}\|^2 \leqslant \|\mathbf{V}^{**}\|^2 = \|\mathbf{S}_0^{**}\|^2 + \underline{\Delta}_i^{x^T} \cdot \underline{\sigma}_i^x. \tag{145}$$

It is recalled that $\|\mathbf{S}\|^2$ is twice the strain energy of the loaded structure; hence for any kinematical and statical superelement meshes, eqns (144) and (145) give upper and lower bounds on the strain energy. If only one force does work during the loading process they also provide bounds on the displacement corresponding to that force.

BOUNDS ON THE LATERAL DISPLACEMENT AT ANY POINT

The main problem of this paper will now be treated: that of finding bounds on the "drift", or horizontal displacement at a particular point of the frame. This quantity is of interest to designers of tall buildings since excessive drift may cause the structure to be unserviceable even while the stresses in the members are well within allowable limits. The hypercircle/superelement method will now be further developed for the purpose of bounding the drift.

It will be recalled[1] that bounds on pointwise quantities associated with the solution S are given by an inner product $\langle \mathbf{S}, \mathbf{G} \rangle$, where G is a suitably chosen state. If the desired quantity is the horizontal displacement at the joint in the upper left corner of the cell labelled (A, I), then the correct choice for G is

$$\mathbf{G} = \mathbf{J}_I^A \tag{146}$$

where reference is made to Fig. 5. If the displacement in the upper right is desired the state $\hat{\mathbf{J}}_I^A$ should be used. Subsequent computations will be based on eqn (146), it being understood that if the "leeward" displacement is desired, $\mathbf{J}_I^A$ should be replaced by $\hat{\mathbf{J}}_I^A$. Now if eqns (115) and (122) are used, G may be written as

$$\mathbf{G} = \frac{1}{4} \sum_{i=1}^{I} H_i \mathbf{D}_i^A = \frac{1}{4} \sum_{i=1}^{I} H_i (\mathbf{Z}_i^A + \hat{\mathbf{Z}}_i^A) \tag{147}$$

so that

$$16\|\mathbf{G}\|^2 = \sum_{i=1}^{I} \sum_{j=1}^{I} H_i H_j (W_{ij}^{AA} + \hat{W}_{ij}^{AA}). \tag{148}$$

It is proposed to apply the bounding formula (82), i.e.

$$\langle \mathbf{C}, \mathbf{G} \rangle - R\|\hat{\mathbf{G}}\| \leqslant \langle \mathbf{S}, \mathbf{G} \rangle \leqslant \langle \mathbf{C}, \mathbf{G} \rangle + R\|\hat{\mathbf{G}}\| \tag{149}$$

in which

$$\|\hat{\mathbf{G}}\|^2 = \|\mathbf{G}\|^2 - \underline{\mathbf{z}}' \cdot \underline{\mathbf{g}}' - \underline{\mathbf{z}}'' \cdot \underline{\mathbf{g}}''. \tag{150}$$

The solution of eqns (90)

$$\underline{\mathbf{K}}\underline{\mathbf{g}}' = \underline{\mathbf{z}}', \quad \underline{\mathbf{B}}\underline{\mathbf{g}}'' = \underline{\mathbf{z}}'' \tag{151}$$

is therefore required. In the above equations

$$\underline{\mathbf{z}}' = \Gamma^{\mathrm{T}}\mathbf{z}', \quad \underline{\mathbf{z}}'' = \Omega^{\mathrm{T}}\mathbf{z}''. \tag{152}$$

The vector $\mathbf{z}'$ is given by eqns (78). In the descriptive notation

$$(\mathbf{z}')_i^x = [\langle \mathbf{U}_i^x, \mathbf{G}\rangle \quad \langle \boldsymbol{\theta}_i^x, \mathbf{G}\rangle \quad \langle \mathbf{V}_i^x, \mathbf{G}\rangle]^{\mathrm{T}}. \tag{153}$$

Now from eqn (146)

$$\langle \mathbf{U}_i^x, \mathbf{G}\rangle = \langle \mathbf{U}_i^x, \mathbf{J}_l^A\rangle = 1 \quad \text{if} \quad \alpha = A, i = l; \quad = 0 \text{ otherwise} \tag{154}$$

and clearly

$$\langle \boldsymbol{\theta}_i^x, \mathbf{G}\rangle = \langle \mathbf{V}_i^x, \mathbf{G}\rangle = 0. \tag{155}$$

Transformations (152) may be written in the form of eqn (110), i.e.

$$(\underline{\mathbf{z}}')_i^{x'} = \Gamma_{ii'}^{xx'}(\mathbf{z}')_{i'}^x \tag{156}$$

and from eqns (153)-(156) it follows that

$$(\mathbf{z}')_i^{x'} = [\Gamma_{ii'}^{Ax'} \quad 0 \quad 0]^{\mathrm{T}}. \tag{157}$$

The vector $\mathbf{z}''$ is similarly given by eqns (78). In the descriptive notation

$$(\mathbf{z}'')_i^x = [\langle \mathbf{R}_i^x, \mathbf{G}\rangle \quad \langle \mathbf{T}_i^x, \mathbf{G}\rangle \quad \langle \mathbf{S}_i^x, \mathbf{G}\rangle]^{\mathrm{T}} \tag{158}$$

and

$$\begin{aligned}
\langle \mathbf{R}_i^x, \mathbf{G}\rangle &= \frac{1}{4}\sum_{j=1}^{J} H_j(\langle \mathbf{R}_i^x, \mathbf{Z}_j^A\rangle + \langle \mathbf{R}_i^x, \hat{\mathbf{Z}}_j^A\rangle) \\
\langle \mathbf{T}_i^x, \mathbf{G}\rangle &= 0 \\
\langle \mathbf{S}_i^x, \mathbf{G}\rangle &= \frac{1}{4}\sum_{j=1}^{J} H_j\langle \mathbf{S}_i^x, \mathbf{Z}_j^A\rangle.
\end{aligned} \tag{159}$$

Now transformations (152) are carried out

$$(\mathbf{z}'')_i^{x'} = \Omega_{ii'}^{xx'}(\mathbf{z}'')_{i'}^x. \tag{160}$$

With these computations the two systems of eqns (151) may be set up and solved. Hence the quantity $\|\hat{\mathbf{G}}\|$ may be determined. The matrices involved in eqns (151) are just the transformed stiffness and flexibility matrices which appear in the vertex equations. Since these latter equations have already been set up and solved, eqns (151) entail relatively little additional effort.

In addition, the inner product $\langle \mathbf{C}, \mathbf{G}\rangle$ appearing in expression (149) is required. From eqn (92c), with $\mathbf{S}_0^* = \mathbf{0}$

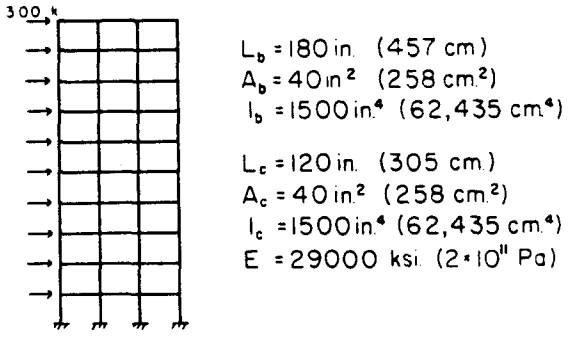

Fig. 9. Structure and loading: example 1.

$$\langle \mathbf{C}, \mathbf{G} \rangle = \tfrac{1}{2}(\underline{\mathbf{z}}' \cdot \underline{\mathbf{x}} + \langle \mathbf{S}_0^{**}, \mathbf{G} \rangle + \underline{\mathbf{z}}'' \cdot \underline{\boldsymbol{\sigma}}). \tag{161}$$

Now from eqns (157) and (102)

$$\underline{\mathbf{z}}' \cdot \underline{\mathbf{x}} = \Gamma_{ii'}^{AA'} \underline{\mathbf{u}}_{i'}^{A'}. \tag{162}$$

If joint (A, I) is a node of the kinematical superelement mesh, eqn (162) becomes simply

$$\mathbf{z}' \cdot \mathbf{x} = \mathbf{u}_I^A. \tag{163}$$

The second term on the right-hand side of eqn (161) is, from eqns (123), (126) and (147)

$$16\langle \mathbf{S}_0^{**}, \mathbf{G} \rangle = \sum_{\alpha=1}^{b} \sum_{i=1}^{n(\alpha)} \sum_{j=1}^{I} H_i H_j (W_{ij}^{\alpha A} q_i^{\alpha} + \hat{W}_{ij}^{\alpha A} \hat{q}_i^{\alpha}). \tag{164}$$

Finally, the last term in eqn (161) must be computed directly from

$$\underline{\mathbf{z}}'' \cdot \underline{\boldsymbol{\sigma}} = (\underline{\mathbf{z}}'')_{i'}^{\alpha'} \underline{\boldsymbol{\sigma}}_{i'}^{\alpha'}. \tag{165}$$

PRACTICAL APPLICATIONS

The computations inherent in the hypercircle/superelement (H/S) method entail no essential difficulty. In order for the method to compete successfully with the conventional matrix displacement approach as a computation tool, however, pains must be taken to eliminate unnecessary operations. This applies especially to transformations (89).

A FORTRAN code, named HYPER, has been created to perform the computations of the H/S method. It has been tailored for analysis of "flattop" frames loaded on their lateral faces as by wind or seismic load. Results obtained with HYPER are now presented and compared with the results of an exact analysis by the conventional matrix displacement (stiffness) method.

The first structure to be studied is the ten story, three bay frame shown in Fig. 9. Three sets of kinematical and statical meshes are used to compute upper and lower bounds on the lateral displacement at the upper left corner of the frame. These mesh pairs are shown in Fig. 10. It is seen that the first mesh pair is extremely coarse while the last mesh pair includes all of the joints and bays of the actual structure. The middle set lies between these two extremes.

Table 1 shows the results obtained from HYPER for the three cases. All of the scalar quantities needed to apply the bounding equation, eqn (82), of the hypercircle method are recorded in Table 1. (For reasons of economy of space the vectors used to compute these

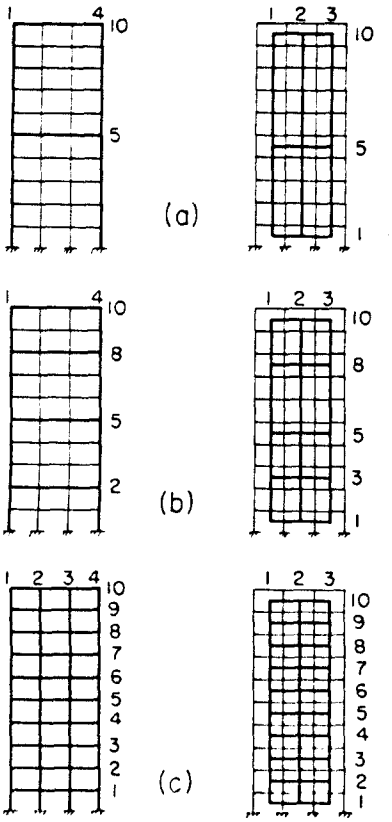

Fig. 10. Kinematical (left) and statical (right) superelement meshes: example 1.

quantities are not listed.) The bounds provided by the coarse meshes are seen to be reasonably close in spite of the small number of degrees of freedom employed ($v' = 12$, $v'' = 27$ compared to $v' = 120$, $v'' = 90$ for the actual structure). Since all the joints and bays of the actual structure are included in the third mesh pair, the bounds coincide and give the exact solution, apart from a small round-off error.

A useful measure of the closeness of the bounds is given by the non-dimensional quantity

$$\underline{R} = R\|\hat{\mathbf{G}}\|/\langle \mathbf{C}, \mathbf{G}\rangle. \tag{166}$$

This may be called the "normalized radius" of the hypercircle. Reference to Table 1 shows that $\underline{R}$ decreases considerably from the first to the second set of meshes. If the requirement $\underline{R} < 0.10$ is adopted as the criterion for calling the bounds "close", then the second set of bounds may be called "close".

In going from the second to the last set of meshes, the expected results

$$\|\mathbf{V}^*\|^2 = \|\mathbf{V}^{**}\|^2 = \|\mathbf{S}\|^2, \quad R = \|\hat{\mathbf{G}}\| = 0, \quad \langle \mathbf{C}, \mathbf{G}\rangle = L = U = u_{\text{actual}} \tag{167}$$

are reflected in the last column of Table 1. The computations were performed by HYPER on an IBM 4341 computer in double precision (64 bit) accuracy. The values of $\|\mathbf{S}\|^2$ and u_{actual} were computed on the same machine by the conventional matrix displacement method.† These agree with the values provided by HYPER to the number of decimal places shown in Table 1. It is also seen that the computed values of R, $\|\hat{\mathbf{G}}\|$, and $\underline{R}$ are essentially zero. The amount of CPU time required for the solution of the above problem by the CMD method is approximately 2.6 s. Reference to the bottom line of Table 1 shows that this is considerably less time than that required by the H/S method even for rough bounds. In

† The linear equation solvers BANFAC and BANSOL due to Weaver and Gere[3] were used in both the CMD method and in HYPER.

Table 1. Results obtained from HYPER for ten story frame example

Mesh	1	2	3	Units
v'/v''	12/27	24/45	120/90	
$\|\mathbf{V}^*\|^2$	5.65730	7.34753	8.41300	k in.
	0.63919	0.830155	0.95054	kN m
$\|\mathbf{V}^{**}\|^2$	10.0960	9.03963	8.41300	k in.
	1.14069	1.02134	0.95054	kN m
$\mathbf{z}' \cdot \mathbf{x}$	0.33446	0.39463	0.43077	in.
	0.84954	1.00236	1.094163	cm
$\mathbf{z}'' \cdot \boldsymbol{\sigma}$	−0.97102	−0.97285	−0.974240	in.
	−2.46640	−2.47105	−2.474570	cm
$\mathbf{z}' \cdot \mathbf{g}'$	0.022318	0.02546	0.027498	in.
	0.056881	0.06466	0.0698460	cm
$\mathbf{z}'' \cdot \mathbf{g}''$	0.06544	0.065542	0.065598	in.
	0.166226	0.166477	0.1666185	cm
$\langle \mathbf{C}, \mathbf{G} \rangle$	0.384226	0.413394	0.430773	in.
	0.975934	1.050021	1.0941634	cm
R	1.05341	0.650373	1.302×10^{-5}	$(\text{k in})^{1/2}$
	11.19714	6.913078	13.84×10^{-5}	$(\text{N m})^{1/2}$
$\|\hat{\mathbf{G}}\|$	0.07304	0.04580	1.477×10^{-6}	$(\text{in. k}^{-1})^{1/2}$
	0.174535	0.10945	3.529×10^{-6}	$(\text{m N}^{-1})^{1/2}$
Lower bound, L	0.30728	0.383606	0.430773	in.
	0.78050	0.974360	1.094163	cm
Upper bound, U	0.46166	0.443182	0.430773	in.
	1.17136	1.125682	1.094163	cm
$\underline{R}$	0.20025	0.07206	4.465×10^{-12}	
CPU time	4.02	4.31	5.17	s

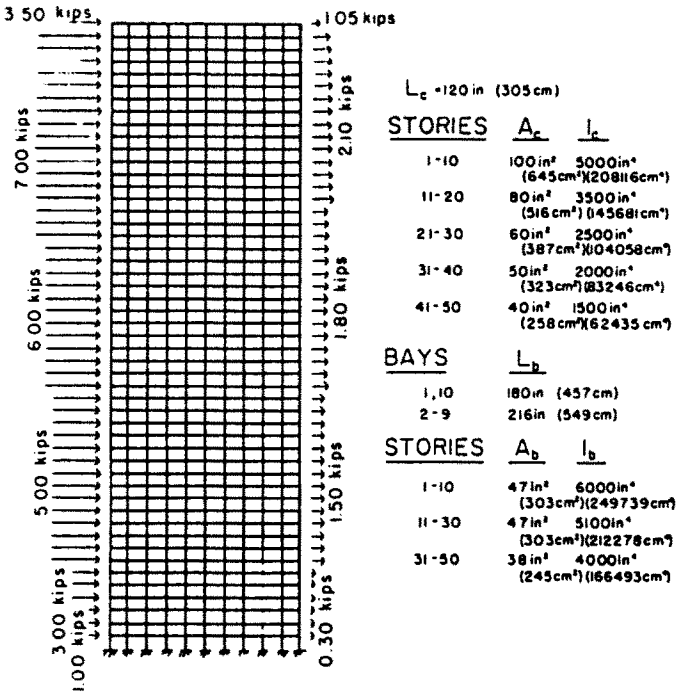

Fig. 11. Structure and loading: example 2.

order for the economy of the new method to be fully appreciated, a very large structure must be considered.

The 50 story, ten bay structure shown in Fig. 11 is used to illustrate the advantage of the H/S method. As indicated in the figure, the beam and column properties change every

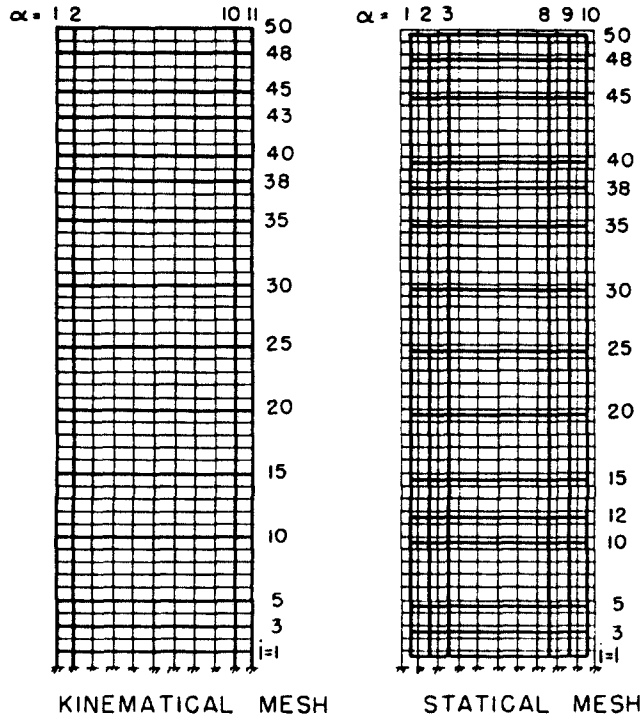

Fig. 12. Mesh 4 of example 2.

Table 2. Superelement meshes for 50-story frame example (case 1, coarsest; case 7, finest)

Mesh	α	i
1, kinematical	1, 11	10, 20, 30, 40, 50
1, statical	1, 2, 9, 10	1, 10, 20, 30, 40, 50
2, kinematical	1, 11	5, 10, 15, 20, 25, 30, 35, 40, 45, 50
2, statical	1, 2, 9, 10	1, 5, 10, 15, 20, 25, 30, 35, 40, 45, 50
3, kinematical	1, 2, 10, 11	5, 10, 15, 20, 25, 30, 35, 40, 45, 50
3, statical	1, 2, 3, 8, 9, 10	1, 5, 10, 15, 20, 25, 30, 35, 40, 45, 50
4, kinematical	1, 2, 10, 11	1, 3, 5, 10, 15, 20, 25, 30, 35, 38, 40, 43, 45, 48, 50
4, statical	1, 2, 3, 8, 9, 10	1, 3, 5, 10, 12, 15, 20, 25, 30, 35, 38, 40, 45, 48, 50
5, kinematical	1, 2, 10, 11	1, 3, 5, 8, 10, 15, 18, 20, 22, 25, 28, 30, 32, 35, 38, 40, 43, 45, 48, 50
5, statical	1, 2, 3, 8, 9, 10	1, 3, 5, 10, 12, 15, 18, 22, 25, 28, 30, 32, 35, 38, 40, 42, 45, 48, 50
6, kinematical	1, 2, 3, 9, 10, 11	1, 3, 5, 8, 10, 15, 18, 20, 22, 25, 28, 30, 32, 35, 38, 40, 43, 45, 48, 50
6, statical	1, 2, 3, 4, 7, 8, 9, 10	1, 3, 5, 10, 12, 15, 18, 20, 22, 25, 28, 30, 32, 35, 38, 40, 42, 45, 48, 50
7, kinematical	1, 2, 3, 9, 10, 11	1, 2, 3, 5, 8, 10, 12, 15, 18, 20, 22, 25, 28, 30, 32, 35, 38, 40, 43, 44, 45, 47, 48, 49, 50
7, statical	1, 2, 3, 4, 7, 8, 9, 10	1, 2, 3, 4, 5, 8, 10, 12, 15, 18, 20, 22, 25, 28, 30, 32, 35, 38, 40, 42, 44, 45, 48, 49, 50

ten stories and the loading also varies with height. The situation pictured is therefore "realistic", although the member properties are not the product of an actual design.

Seven sets of superelement meshes (Fig. 12), numbered 1–7 in order of increasing fineness, are defined in Table 2. The essential results of the H/S analysis of the seven cases, using HYPER, are given in a graphical representation by Figs 13 and 14. Details are given in Table 3. Figure 13 shows the convergence of $\|\mathbf{V}^*\|^2$ and $\|\mathbf{V}^{**}\|^2$ to the value of $\|\mathbf{S}\|^2$. It is seen that the energy of the state $\mathbf{V}^*$ converges rapidly as the number of degrees of freedom is increased while $\|\mathbf{V}^{**}\|^2$ approaches the true value somewhat more slowly. As the theory demands, each successive refinement of the kinematical and statical superelement meshes drives $\|\mathbf{V}^*\|^2$ higher and $\|\mathbf{V}^{**}\|^2$ lower. The question of how exactly to achieve the best values for a given number of degrees of freedom will not be explored here. (Indeed, one of the virtues of the H/S method is that any reasonable meshes will yield reasonable

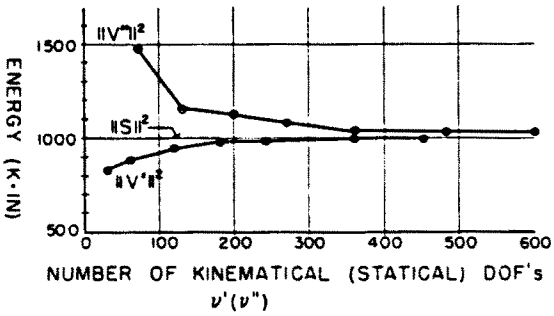

Fig. 13. Convergence behavior of energy bounds: example 2.

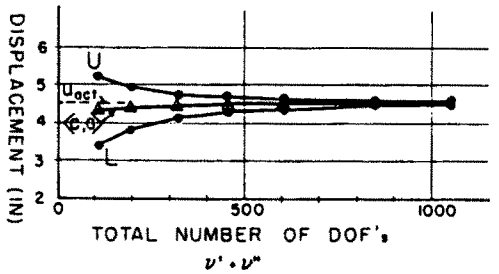

Fig. 14. Convergence behavior of drift bounds: example 2.

Table 3. Results obtained from HYPER for 50-story frame example

Mesh	1	2	3	4	5	6	7	Units
ν'/ν''	30/72	60/132	120/198	180/270	240/360	360/480	450/600	
$\|V^*\|^2$	826.949	881.043	942.058	980.198	981.411	955.442	996.104	k in.
	93.4323	99.5440	106.438	110.747	110.884	112.469	112.544	kN m
$\|V^{**}\|^2$	1479.97	1156.15	1125.21	1080.16	1035.38	1030.37	1022.02	k in.
	167.214	130.626	127.131	122.041	116.982	116.415	115.472	kN m
$z'\cdot x$	3.91714	4.05925	4.33927	4.44719	4.44810	4.53487	4.53690	in.
	9.94953	10.3105	11.0217	11.2959	11.2982	11.5186	11.5237	cm
$z''\cdot\sigma$	−232.337	−232.331	−232.467	−232.474	−232.472	−232.502	−232.511	in.
	−590.135	−590.120	−590.466	−590.484	−590.478	−590.556	−590.579	cm
$z'\cdot g'$	0.023885	0.024570	0.026302	0.026775	0.026808	0.027449	0.027535	in.
	0.060668	0.062407	0.066807	0.068007	0.068093	0.069722	0.069940	cm
$z''\cdot g''$	2.00465	2.00468	2.00560	2.00563	2.00564	2.00584	2.00594	in.
	5.09181	5.09188	5.09423	5.09430	5.09431	5.09484	5.09508	cm
$\langle C, G\rangle$	4.32516	4.39971	4.47096	4.52153	4.52301	4.55123	4.54769	in.
	10.9858	11.1752	11.3562	11.4847	11.4885	11.5601	11.5511	cm
R	12.7772	8.29313	6.76661	4.99900	3.67327	2.95490	2.5452	$(k\ in.)^{1/2}$
	135.814	88.1510	71.9250	53.1364	39.0447	31.4089	27.054	$(N\ m)^{1/2}$
$\|\bar{G}\|$	0.07186	0.06671	0.04236	0.03591	0.03540	0.0201	0.0150	$(in.\ k^{-1})^{1/2}$
	0.17171	0.15942	0.10122	0.08582	0.08459	0.0480	0.0359	$(m\ N^{-1})^{1/2}$
L	3.40702	3.84580	4.18433	4.34199	4.39298	4.49185	4.50945	in.
	8.65383	9.76834	10.6282	11.02866	11.1582	11.4093	11.45400	cm
U	5.24331	4.95235	4.75758	4.70106	4.65305	4.61062	4.58594	in.
	13.3180	12.5790	12.0842	11.9407	11.8187	11.7110	11.6483	cm
$\underline{R}$	0.21228	0.12577	0.064108	0.03971	0.028749	0.01305	0.008410	
CPU time	35.74	36.64	36.63	38.21	39.15	43.47	46.21	s

bounds.) It is possible, however, to make certain observations concerning the effect of adding additional lines of nodes to the meshes. In going from case 4 to case 5, for example, the extra horizontal nodal lines cause $\|V^{**}\|^2$ to decrease markedly but have a relatively small effect on $\|V^*\|^2$. On the other hand, in going from case 5 to case 6, the added vertical nodal lines cause a large increase in $\|V^*\|^2$ and only a small decrease in $\|V^{**}\|^2$. It is anticipated that the analyst who uses the H/S method will develop a sense of how to construct superelement meshes for bounds of a desired closeness.

The upper and lower bounds provided by HYPER are shown in Fig. 14 as a function of the total number of degrees of freedom (DOF), $\nu'+\nu''$, for each of the seven sets of

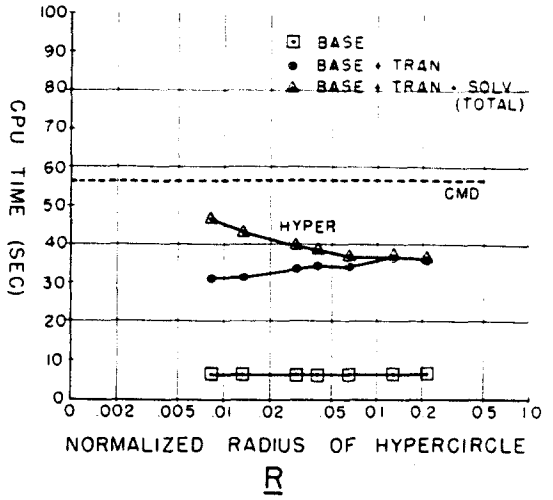

Fig. 15. Computer time required by hypercircle method as function of bound width: comparison with conventional matrix displacement method.

meshes. The value of $\langle \mathbf{C}, \mathbf{G} \rangle = \frac{1}{2}(L+U)$ is also shown. It may be noted that $\langle \mathbf{C}, \mathbf{G} \rangle$ provides a good approximation of the drift and initially approaches u_{actual} from below. It should be remembered, however, that $\langle \mathbf{C}, \mathbf{G} \rangle$ is not theoretically guaranteed to represent either a lower or an upper bound on the displacement.

It is now appropriate to examine the critical question of computer time. Figure 15 shows the CPU time required by HYPER to achieve certain values of R for the seven sets of meshes. (The significance of the three different curves below HYPER will be discussed below.) The time required by the conventional matrix displacement method (CMD) is shown as a horizontal dashed line. It is seen immediately that HYPER is faster than the CMD method even when very small values of R are required. In fact, for the finest mesh used it is found that $R < 0.01$ and the time required is still well below that required by the conventional matrix displacement method. An equally important observation is that the computational effort of the new method rises at a relatively slow rate over a wide range of values of R, extending well into the region required for "close" bounds. This remarkable feature of the H/S method is discussed in more detail below. While it is clear that for sufficiently small values of R the HYPER curve must intersect the CMD curve, it is also obvious that, for this type of problem at least, the bounds may be narrowed very far without any large increase in computer time.

In order better to understand this behavior, a simple analysis may be carried out by considering a square frame having N column lines and N beam lines. (To simplify matters the ground line is treated as a beam line.) If a uniform kinematical superelement mesh having ν horizontal and vertical lines of nodes is assumed, then the number of multiplications required to carry out transformation $(89)_1$, i.e.

$$\mathbf{K} = \mathbf{\Gamma}^{\mathrm{T}} \mathbf{K} \mathbf{\Gamma} \tag{168}$$

may be determined as follows. Equation (168) is first rewritten

$$\mathbf{K}_{i'j'}^{\alpha'\beta'} = \sum_{\alpha=1}^{N} \sum_{\beta=1}^{N} \sum_{i=1}^{N} \sum_{j=1}^{N} \Gamma_{ii'}^{\alpha\alpha'} \Gamma_{jj'}^{\beta\beta'} \mathbf{K}_{ij}^{\alpha\beta} \qquad \alpha', \beta', i', j' = 1, \nu. \tag{169}$$

Due to the sparseness of the matrices involved, only a small number of the multiplications yield non-zero products. Furthermore, the symmetry of $\underline{\mathbf{K}}$ requires only the computation of five matrices for each node (α', i')

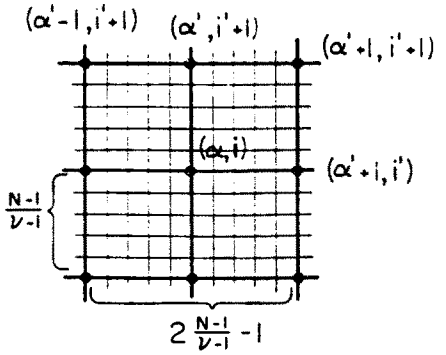

Fig. 16. Nodes associated with $\underline{\mathbf{K}}$ matrices.

$$\underline{\mathbf{K}}^{\alpha'\alpha'}_{i'i'},\ \underline{\mathbf{K}}^{\alpha'(\alpha'+1)}_{i'i'},\ \underline{\mathbf{K}}^{\alpha'(\alpha'-1)}_{i'(i'+1)},\ \underline{\mathbf{K}}^{\alpha'\alpha'}_{i'(i'+1)},\ \underline{\mathbf{K}}^{\alpha'(\alpha'+1)}_{i'(i'+1)}. \tag{170}$$

The nodes associated with each of these five matrices are shown in Fig. 16. To compute $\underline{\mathbf{K}}^{\alpha'\alpha'}_{i'i'}$, the number of multiplications required is $(2)(5)\{[2(N-1)/(\nu-1)]-1\}^2$, where the factor in curly brackets squared is the number of joints (α, i) for which the factor $\Gamma^{\alpha\alpha'}_{ii'}$ does not vanish, and the factor 5 is the number of nodes (β, j) associated with each (α, i) for which $\mathbf{K}^{\alpha\beta}_{ij}$ is a non-zero matrix. If a similar analysis is carried out for the other four matrices in (170) it is found that the total number of multiplications required for transformation (169) is

$$M = 10\nu^2(10\lambda^2 - 6\lambda + 1) \tag{171}$$

where $\lambda = (N-1)/(\nu-1)$.

This may be approximated closely by

$$M \simeq 10\nu^2[(10)^{1/2}\lambda - 1]^2. \tag{172}$$

Differentiation of this expression with respect to ν then shows that

$$\mathrm{d}M/\mathrm{d}\nu \simeq 20\nu[(10)^{1/2}\lambda - 1]\{[(10)^{1/2}\lambda/(1-\nu)] - 1\} \tag{173}$$

which is clearly negative. It may be concluded that, for the idealized problem formulated above, the number of multiplications required for transformation (168) decreases as the uniform mesh is made finer. It should be noted that no provision has been made for nodes that lie on the boundary of the structure; hence the analysis holds strictly only for very large frames with relatively fine meshes.

Now the results presented in Fig. 15 may be understood clearly. The lowest curve below HYPER represents the basic computational effort; it is independent of the nature of the superelement meshes (computation of $\mathbf{K}$, $\mathbf{B}$, $\mathbf{P}$, Δ, $\|\mathbf{S}^{**}_0\|^2$, $\|\mathbf{G}\|^2$, etc.). The second curve represents the basic computations plus those associated with transformations (89) giving $\underline{\mathbf{K}}$, $\underline{\mathbf{B}}$, etc. It is observed that this curve tends generally downward with decreasing values of $\underline{R}$. This is exactly the behavior predicted by eqn (173); i.e. $\underline{\mathbf{K}}$ and $\underline{\mathbf{B}}$ require less computation as the kinematical and statical superelement meshes are made finer. Due to this behavior the total CPU time required by HYPER does not begin to increase significantly until the vertex equations, eqns (87), become large enough so that their solution requires more time than is saved in their formulation. Accordingly, the uppermost curve in Fig. 15 shows that there is a "window" at the right-hand end in which $\underline{R}$ may be decreased without any significant increase in CPU time.

CONCLUSIONS

This work consists of two parts. Part I[1] develops the theoretical background for the application of the hypercircle method to frame analysis. In Part II, the theory of the hypercircle is applied to rigid-jointed plane frames composed of horizontal beams and vertical columns. A superelement method is introduced to reduce the number of kinematical and statical degrees of freedom of the structure while creating subspaces that pass as closely as desired to the actual solution. To test the usefulness of the new method as a tool for determining upper and lower bounds on the "drift" of tall buildings, two structures are studied. It is found that the hypercircle/superelement method of analysis gives useful bounds even for relatively coarse superelement meshes. For a 50-story, ten bay frame the new method provides close bounds in significantly less time than is required by the conventional matrix displacement approach.

Acknowledgement—One of us (C.A.N.) acknowledges with thanks the support of the Department of Civil Engineering, University of Manitoba, Canada.

REFERENCES

1. C. A. Nelson and L. E. Goodman, Hypercircle method in frame analysis—I. Theory. *Int. J. Solids Structures* **24**, 619–636 (1988).
2. R. H. Gallagher, *Finite Element Analysis*, p. 224 *et seq.* Prentice-Hall, Englewood Cliffs, New Jersey (1975).
3. W. Weaver, Jr. and J. M. Gere, *Matrix Analysis of Framed Structures*, 2nd Edn, pp. 467–472. Van Nostrand Reinhold, New York (1980).

APPENDIX. NOTATION

$\mathbf{B}_{ij}^{\alpha\beta}$	3×3 matrix of inner products of basic residual states
$\mathbf{B}_{ij}^{\alpha'\beta'}$	transformed matrix of inner products
$\mathbf{D}_i^{\alpha}, \hat{\mathbf{D}}_i^{\alpha}$	states used in construction of $\mathbf{S}_{ij}^{\alpha\beta}$; see eqns (115)
$\mathbf{g}_i', \mathbf{g}_i''$	transformed vectors used in computation of $\|\mathbf{G}\|$, defined as solution of eqns (151)
$\mathbf{J}_i^{\alpha}, \hat{\mathbf{J}}_i^{\alpha}$	states resulting from unit pressure and suction loads at ith story of αth bay (Fig. 11)
$\mathbf{K}_{ij}^{\alpha\beta}$	3×3 matrices of inner products of basic compatible states
$\mathbf{K}_{ij}^{\alpha'\beta'}$	transformed matrices of inner products
H_i, L_α	height of ith story, length of αth bay
$N_{ir}, N^{\alpha s}$	one-dimensional linear shape functions in the vertical and horizontal directions, defined by eqns (105) and (106)
$P_i^{\alpha}, \hat{P}_i^{\alpha}$	pressure and suction loads acting at ith story of αth bay
$q_i^{\alpha}, \hat{q}_i^{\alpha}$	quantities used in computation of $\|\mathbf{S}_{ij}^{\alpha\beta}\|$, defined by eqns (124)
$\mathbf{R}_i^{\alpha}, \mathbf{T}_i^{\alpha}, \mathbf{S}_i^{\alpha}$	basic residual states associated with cell (α, i)
$r_i^{\alpha}, t_i^{\alpha}, s_i^{\alpha}$	redundant forces associated with basic residual states
$\mathbf{U}_i^{\alpha}, \mathbf{V}_i^{\alpha}, \boldsymbol{\theta}_i^{\alpha}$	basic compatible states associated with joint (α, i)
$u_i^{\alpha}, v_i^{\alpha}, \theta_i^{\alpha}$	joint displacements associated with basic compatible states
$W_{ij}^{\alpha\beta}, W_{ij}^{\alpha'\beta'}$	inner products of the states $Z_i^{\alpha}, Z_j^{\beta}$; defined by eqns (126)
$\mathbf{x}_j^{\beta}$	vector of joint displacements associated with joint (β, j)
$\mathbf{x}_j^{\beta'}$	transformed vector of joint displacements
$\mathbf{Z}_i^{\alpha}, \hat{\mathbf{Z}}_i^{\alpha}$	states used in construction of $\mathbf{S}_{ij}^{\alpha\beta}$, defined by eqns (122)
$(\mathbf{z}')_i^{\alpha}, (\mathbf{z}'')_i^{\alpha}$	vectors defined by eqns (153) and (158)
$(\mathbf{z}')_i^{\alpha'}, (\mathbf{z}'')_i^{\alpha'}$	vectors obtained from transformations (152)
Δ_i^{α}	right-hand side vectors of force equations, defined by eqn (131)
$\Delta_i^{\alpha'}$	transformed right-hand side vectors of force equations
$\Gamma_{ir}^{\alpha s}$	matrices of two-dimensional shape functions associated with kinematical superelement mesh
$\Omega_{ir}^{\alpha s}$	matrices of two-dimensional shape functions associated with statical superelement mesh
$\Pi_i^{\alpha}, \hat{\Pi}_i^{\alpha}$	sum of pressure, suction loads acting on αth bay from ith story to top of bay
$\boldsymbol{\sigma}_j^{\beta}$	vector of redundant forces associated with cell (β, j)
$\boldsymbol{\sigma}_j^{\beta'}$	transformed vector of redundant forces.